Solitary waves in a chain of beads under Hertz contact

C. Coste, E. Falcon, and S. Fauve

Laboratoire de Physique, Ecole Normale Superieure de Lyon, URA CNRS 1325, 46 Allée d'Italie,
69364 Lyon Cedex 07, France

We study experimentally the propagation of high-amplitude compressional waves in a chain of beads in contact, submitted or not to a small static force. In such a system, solitary waves have been theoretically predicted by Nesterenko [J. Appl. Mech. Tech. Phys. (USSR) **5**, 733 (1984)]. We have built an impact generator in order to create high-amplitude waves in the chain. We observe the propagation of isolated nonlinear pulses, measure their velocity as a function of their maximum amplitude, for different applied static forces, and record their shape. In all experiments, we find good agreement between our observations and the theoretical predictions of the above reference, without using *any* adjustable parameter in the data analysis. We also show that the velocity measurements taken at three different nonzero applied static forces all lie on a single curve, when expressed in rescaled variables. The size of the pulses is typically one-tenth the total length of the chain. All the measurements support the identification of these isolated nonlinear pulses with the solitary waves predicted by Nesterenko. [S1063-651X(97)04211-6]

PACS number(s): 03.40.Kf, 46.10.+z, 43.25.+y

I. INTRODUCTION

Granular materials are widely spread in both geophysical and industrial contexts. Acoustic waves are frequently used as nondestructive testing tools in the laboratory and are sometimes the only accessible way to get information in geophysical investigations. Thus the acoustic behavior of granular materials has been widely investigated for a long time [1,2].

The shape of the grains, the details of the contact law between adjacent grains, the geometry of the contact lattice, and hence the dimensionality of the grain piling all affect the propagation of sound in granular material. This variety of phenomena makes the problem difficult and many open questions subsist (see [3] for a recent review). Many experimental investigations were concerned with the propagation of seismic waves in materials submitted to very high pressures [4–6], where all those problems are somewhat mixed. Recent works on sound propagation in sand focus on geometrical effects due to the disorder of the piling [7,8]. In this paper we are concerned with the effect of the contact law between adjacent grains and the resulting nonlinear and dispersive behaviors.

The interaction law between two adjacent elastic spheres is an exact solution of linear elasticity, known as Hertz's law [9]. Because of purely geometrical effects, the relation between the force F_0 exerted on the spheres and the distance of approach of their centers δ_0 is nonlinear, $F_0 \propto \delta_0^{3/2}$. As a consequence of Hertz's interaction law, the velocity of linear sound waves in one-dimensional systems scales as $F_0^{1/6}$; this classical result, experimentally demonstrated long ago [1,2] (for more recent results see [10]), does not seem to be verified in higher dimensions because of geometrical effects [3]. To get rid of such problems, a one-dimensional ordered system such as a chain of identical elastic beads is a good candidate to study the nonlinear regime.

The nonlinear behavior of a chain of beads was originally investigated with the help of numerical simulations, in order to study the propagation of *shock waves* in the chain, for several nonlinear interaction laws [11–13]. Nesterenko [14,15] gave an analytical solution to the problem for Hertz's law. He showed that strong compressional waves, that is, with an amplitude much greater than the applied static force, may propagate as isolated *solitary waves* in the chain. Later, experimental evidence of the existence of such waves was given by Nesterenko and Lazaridi [16–18]. A strongly related problem, if not exactly identical, is the propagation of waves in a vertical column of grains subjected to gravity, which is crucial to the understanding of the details of the whole column dynamics after an impact [19,20].

In this paper we report quantitative experiments on nonlinear wave propagation in a chain of identical elastic beads, allowing a comparison of the shape and the velocity of the waves with the theoretical predictions of Ref. [14]. We observe the propagation of nonlinear isolated pulses and a detailed analysis, in which no free adjustable parameter is used, strongly supports their identification with the solitary waves described by Nesterenko [14]. Our experimental setup allows a systematic study of the waves in a large range of amplitudes for several applied static forces. This is in contrast with the work of Refs. [16, 17], in which the excitation of the waves cannot be varied and only indirect velocity measurements were performed.

The paper is organized as follows. In Sec. II we review the calculations of Nesterenko for convenience and further reference. Section III A is devoted to the presentation of our experimental apparatus and Sec. III B to the analysis of the data and a comparison with the theoretical predictions. The experimental results are presented in Sec. IV. We display the experimental shape of the nonlinear pulses in Sec. IV A for a chain submitted to moderate static forces (29.4 and 167 N). In Sec. IV B we report on measurements of the velocity of propagation of the nonlinear pulses for three different applied static forces (9.8, 29.4, and 167 N). We show that when the velocity is rescaled by the *linear* sound velocity and the maximum amplitude of the pulses is rescaled by the applied

static force, the previous measurements all lie on a single curve. Section IV C is devoted to the behavior of a chain in the absence of any static force because the theoretical status of this case is somewhat singular. In Sec. IV D we discuss our results in the light of previous works [16–18]. Our conclusions are given in Sec. V.

II. THEORETICAL ANALYSIS

When two identical elastic spheres of radius a are in contact and submitted to a *static* force F_0, the distance of approach δ_0 of their centers reads

$$\delta_0 = \frac{2(\theta F_0)^{2/3}}{a^{1/3}} \quad \text{with} \quad \theta \equiv \frac{3(1-\nu^2)}{4E}, \tag{1}$$

where E is Young's modulus and ν Poisson's ratio of the bead material. This is an exact result of *linear* elasticity, known as Hertz's solution [9], and the nonlinear relationship between δ_0 and F_0 is a purely geometrical effect.

This solution is expected to remain valid when the force F and hence the distance of approach δ are both slowly varying functions of time. The variations may be considered as slow if every typical time scale involved in the motion is much greater than the time needed by a bulk longitudinal acoustic wave to travel across the diameter of a bead. For the stainless-steel beads used in our experiments, which are 8 mm in diameter, this condition is fulfilled when all time scales are much greater than 2 μs or all frequencies much less than 500 kHz. Figures 6–8 and 13–15 below show that it is indeed the case in all our experiments. Moreover, the deformation of the beads in contact is strongly confined to a very small region near the contact point; it is thus possible to model a chain of identical beads in contact as a chain of point masses $m = 4\pi\rho a^3/3$, where ρ is the density of each bead, linked by nonlinear springs governed by Eq. (1). The dynamics of the chain, at sufficiently low frequencies, is thus described by the system of coupled nonlinear differential equations

$$\ddot{u}_n = \frac{\sqrt{a/2}}{2m\theta} \{ [\delta_0 - (u_n - u_{n-1})]^{3/2} - [\delta_0 - (u_{n+1} - u_n)]^{3/2} \}, \tag{2}$$

where u_n is the displacement of the nth bead from its equilibrium position and $\ddot{u}_n$ its second time derivative.

Two other approximations are hidden in Eq. (2). First, plastic deformation of the beads is neglected. The nonlinear waves are generated by impacting the first bead of the chain with a bead of maximum speed roughly 0.5 m/s (see Sec. III A). For steel beads, plastic deformation is negligible if the relative speed of the impacting bodies is less than 1.3 m/s [21], so that this effect is actually not relevant to our experimental situation. Dissipation of the waves may also occur because of the viscoelastic behavior of the bead material [22], but this effect is presumably very small for steel beads, and we neglect it too. The validity of those approximations is checked experimentally, *a posteriori*. In the limit of very small amplitude waves, for which the plastic effects are not relevant, the behavior of the chain is very well accounted for by the dissipationless model (2) [10]. In the strongly nonlinear regime, there is very good agreement between the theo-

retical predictions, which do not take dissipative phenomena into account, and the observations (see Sec. IV).

The linear approximation of Eq. (2), obtained in the limit $|u_n - u_{n-1}| \ll \delta_0$, gives for the linearized spring constant

$$k \equiv \left(\frac{\partial \delta_0}{\partial F_0} \right)^{-1} = \frac{3}{4} \frac{(aF_0)^{1/3}}{\theta^{2/3}} \tag{3}$$

and we recover the well-known results for a chain of identical point masses linked by identical linear springs. The dispersion relation between the wave number q and the pulsation ω is

$$\omega = 2\sqrt{\frac{k}{m}} |\sin(qa)|, \tag{4}$$

the cutoff frequency f_c of the chain reads

$$f_c = \frac{1}{\pi} \sqrt{\frac{k}{m}} = \frac{3}{4\pi^{3/2}} \frac{F_0^{1/6}}{\theta^{1/3} a^{4/3} \rho^{1/2}}, \tag{5}$$

and the sound velocity c_s of the chain, not to be confused with the velocities of acoustic waves in the bulk material of the beads, is given by

$$c_s \equiv \lim_{q \to 0} \frac{\omega}{q} = 2a\sqrt{\frac{k}{m}} = \frac{3}{2\sqrt{\pi}} \frac{F_0^{1/6}}{\theta^{1/3} a^{1/3} \rho^{1/2}}. \tag{6}$$

The simple results (5) and (6) are of course well known (see, e.g., [3]) and were recently tested for an actual chain of identical elastic beads [10]. They both have been confirmed experimentally with a great accuracy; this constitutes a clear experimental proof of the validity of the approximations leading to Eq. (2), which are otherwise rather uncontrolled. We will return to the same tests in the nonlinear regime in Sec. IV.

An interesting feature displayed by Eq. (6) is that without any static force $F_0 = 0$, no linear acoustic waves propagate in the chain: $c_s = 0$. Nesterenko [14] called this situation the *sonic vacuum*. He also showed that strongly nonlinear waves do propagate, even when the beads are just in contact, but in the absence of any static force. For convenience and further reference, we reproduce below his analysis, which may be found in [14].

The strongly nonlinear limit corresponds to $|u_n - u_{n-1}| \gg \delta_0$. In the long-wavelength approximation, that is, when the characteristic size L of the perturbation is much greater than the radius of a bead, we may write $u_n(t) = u(x,t)$, where x represent the abscissa along the chain, and proceed to the development

$$u_{n\pm1}(t) = u(x \pm 2a, t) = u \pm 2au_x + 2a^2 u_{xx} \pm \frac{4a^3}{3} u_{xxx}$$

$$+ \frac{2a^4}{3} u_{xxxx} + \cdots, \tag{7}$$

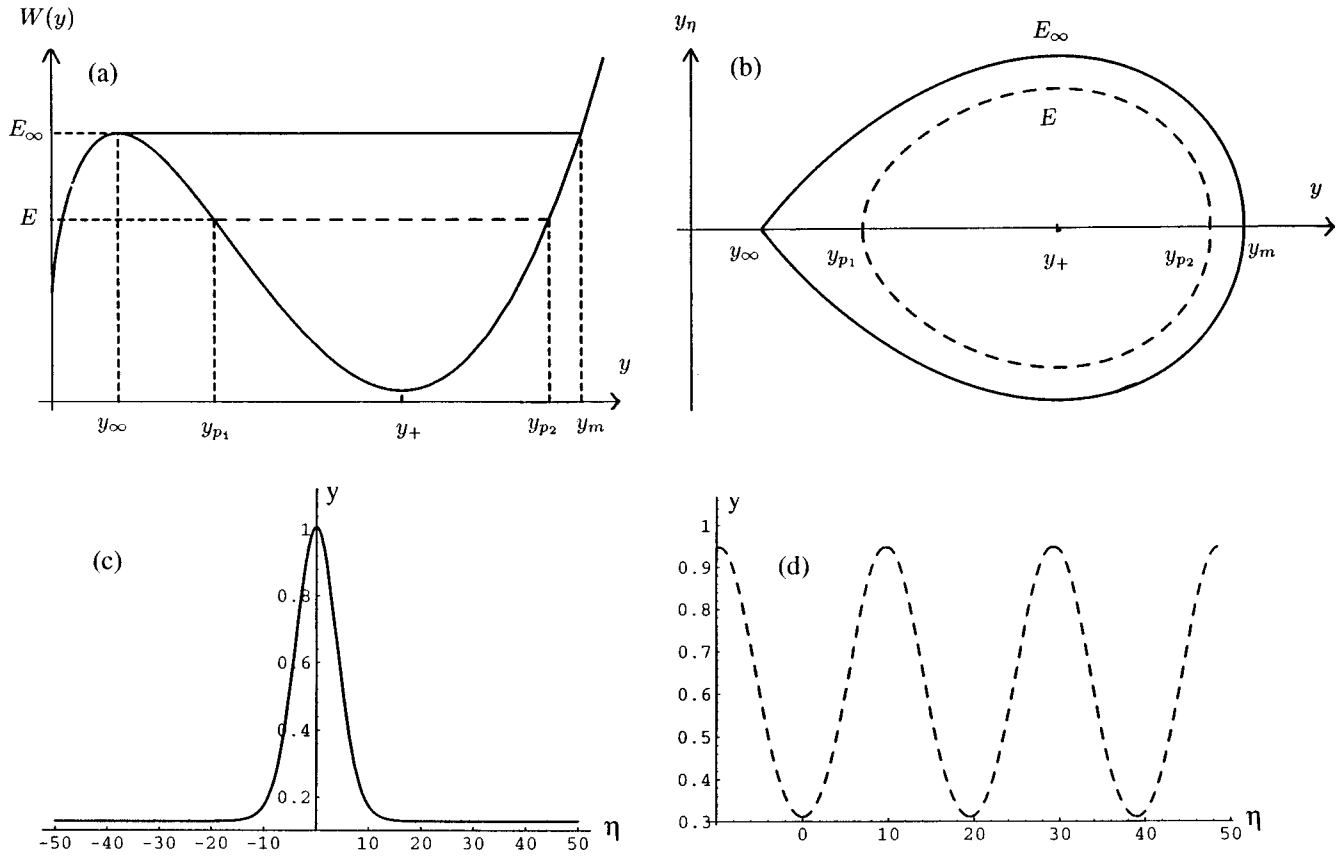where $u_x = \partial u/\partial x$. Inserting this development in Eq. (2), we get

FIG. 1. (a) Graph of the function $W(y)$, illustrating the mechanical analogy between the solutions of Eq. (11) and the motion of a point particle of unit mass in a potential $W(y)$; the parameter of the graph is $y_\infty = 0.128$, which means $y_m = 1.007$. The motion of the particle with energy $E_\infty = 0.011$ corresponds to the solitary wave solution of Eq. (11). Also shown is a particle of energy $E = 0.005$, corresponding to a nonlinear periodic wave solution of Eq. (11). (b) Same as (a), but the respective motions are shown in the phase plane (y, y_η); the homoclinic orbit (solid line) corresponds to the solitary wave, the periodic orbit (dashed line) to the nonlinear periodic wave. (c) Shape of the solitary wave corresponding to the motion of the particle with energy E_∞. (d) Shape of the nonlinear periodic wave corresponding to the motion of the particle with energy E.

$$u_{tt} = C^2 \left[\frac{3}{2}(-u_x)^{1/2}u_{xx} + \frac{a^2}{2}(-u_x)^{1/2}u_{xxxx} - \frac{a^2 u_{xx}u_{xxx}}{2(-u_x)^{1/2}} \right.$$

$$\left. - \frac{a^2}{16}\frac{(u_{xx})^3}{(-u_x)^{3/2}} \right], \quad -u_x > 0, \quad C^2 \equiv \frac{2a^3}{m\theta}, \quad (8)$$

where u is now the *total* displacement of the bead center from its position when no static force is applied. Equation (8) is valid up to order $(a/L)^2$. Looking for progressive waves $u(\xi \equiv x - Vt)$, where the wave velocity V remains to be determined, and setting $\psi = -u_\xi$, we transform Eq. (8) into

$$\frac{V^2}{C^2}\psi_\xi = \frac{3}{2}\psi^{1/2}\psi_\xi + \frac{a^2}{2}\frac{(\psi\psi_{\xi\xi})_\xi}{\psi^{1/2}} - \frac{a^2}{16}\frac{\psi_\xi^3}{\psi^{3/2}}. \quad (9)$$

This equation may be integrated and put in dimensionless form with the help of successive changes of variables

$$\psi = z^{4/5}, \quad z = \left(\frac{V}{C}\right)^5 y, \quad \xi = \sqrt{\frac{2}{5}}\,a\eta, \quad (10)$$

so that we finally get a particularly simple expression

$$y_{\eta\eta} = -\frac{d}{dy}W(y)$$

with

$$W(y) = -\frac{5}{8}y^{8/5} + \frac{1}{2}y^2 + \frac{5}{4}(y_\infty^{4/5} - y_\infty^{6/5})y^{4/5}, \quad (11)$$

where y_∞ is the value taken by y when $\eta \to \pm\infty$. The integration constant is such that $y_{\eta\eta}|_{\pm\infty} = 0$, which means that the solution will have the form of a localized excitation. The function $W(y)$ has a maximum for $y = y_\infty$ and a minimum for

$$y_+ = \left\{ \frac{1}{2}\left[1 - y_\infty^{2/5} + \sqrt{(1 - y_\infty^{2/5})(1 + 3y_\infty^{2/5})}\right] \right\}^{5/2}, \quad (12)$$

defined for $0 \leq y_\infty \leq 1$; moreover, $y_+ \geq y_\infty$ for $0 \leq y_\infty \leq (\frac{2}{3})^{5/2}$. Thus, when y_∞ belongs to this last range, the curve $W(y)$ has the shape displayed in Fig. 1(a).

Equation (11), in an obvious mechanical analogy, describes the motion of a particle of unit mass at position y, in the potential $W(y)$, during the time η. If the particle is initially at the position y_∞, with energy E_∞, it leaves its unstable equilibrium position up to position y_m, defined by
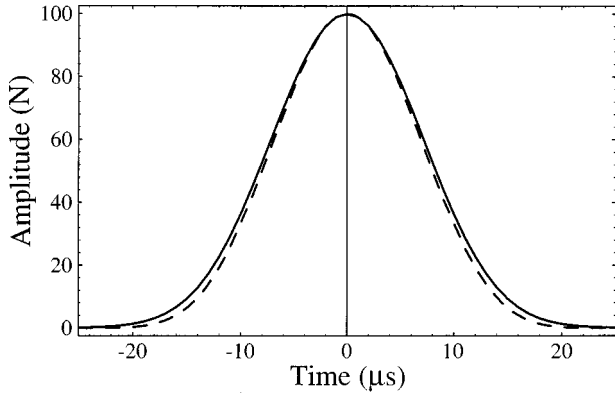
$$W(y_m) - W(y_\infty) = 0, \quad (13)$$

FIG. 2. Evolution of the force (in N) as a function of time (in μs) for a maximum amplitude of 100 N and, respectively, a static force of 1 N (solid line) [the wave profile is determined by Eq. (23)] and no static force (dashed line) [the wave profile is determined by Eq. (28)]. The similarity of the two curves is striking; the choosen value of 1 N roughly corresponds to the available resolution on the static force (see Sec. III A).

in an infinite time because y_∞ is the location of a maximum of the potential, and then returns to position y_∞ again in an infinite time; the corresponding trajectory in the phase plane (y, y_η) is a homoclinic orbit [see Fig. 1(b)]. Returning to our wave problem, this describes the propagation of a solitary wave of amplitude y_∞ at $\eta \to \pm\infty$ and of maximum amplitude y_m at $\eta = 0$, say; the shape of a typical wave profile is displayed in Fig. 1(c). Also shown in Fig. 1(d) is a solution of energy $E < E_\infty$, represented by the dashed closed orbit in the phase plane, and corresponding to a nonlinear periodic wave.

Those conclusions are valid for $y_\infty > 0$ because the change of variables (10) is singular for $y = 0$. The solution for $y_\infty = 0$, which corresponds physically to $F_0 = 0$, is a nonlinear periodic wave train [14] with an analytic expression that reads, in the original variables ψ and ξ,

$$\psi(\xi) = \left(\frac{5}{4} \frac{V^2}{\mathcal{C}^2} \right)^2 \cos^4 \frac{\xi}{a\sqrt{10}}. \tag{14}$$

This solution is mathematically singular because it does not fulfill the inequality $\psi = -u_\xi > 0$ [see (8)]. On the other hand, those nonlinear periodic waves are *modulationally stable*, as shown in Ref. [23], so that they may be relevant to the actual behavior of the chain. Experimentally, it seems that solitary waves exist also when no static force is applied to the chain (see [16,17] and Sec. IV C). It is very unlikely that a qualitative change suddenly appears at zero static force because solitary waves exist at any infinitesimal applied static force. The shape of a solitary wave with a small static force is extremely similar to one arch of the nonlinear wave (14), as shown by Fig. 2. This behavior is confirmed by numerical simulations of Nesterenko and Lazaridi [17,18], who found the same properties for a wave of maximum amplitude 200 N propagating either under a static force of 2 N or in an uncompressed chain. Moreover, the wave velocity also tends continuously toward its zero static force limit, as shown in Sec. III B. We return to the theoretical status of
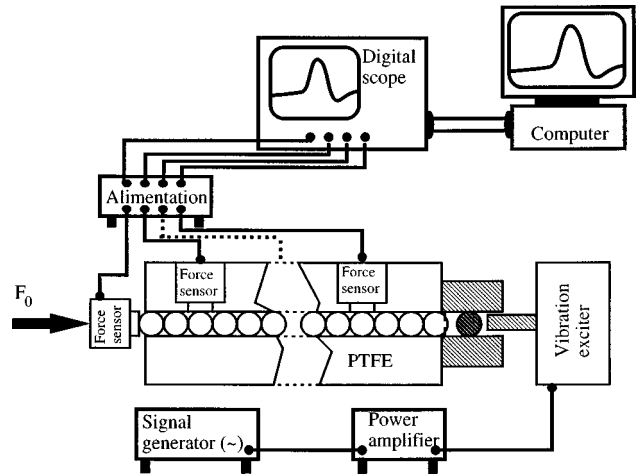

FIG. 3. Sketch of the experimental apparatus (not to scale). The framework of PTFE consists of two parts, each one 30 mm high, 40 mm wide and 400 mm long, with a straight channel of squared cross section, 8.02-mm sides, milled in the lower part, that contains the beads. A very small clearance of 2/100 mm is managed in the channel, so that the beads move freely along the axis but not in the perpendicular direction. Only two of the sensors perpendicular to the chain axis are shown as well as the one that is parallel to the chain axis; they are all piezoelectric quartz transducers with charge amplifiers included hence the need of a stabilized electrical alimentation. The impact generator is described in Fig. 4. Two mechanical devices, not represented here, ensure longitudinal (i.e., parallel to the chain axis) displacement of both the dynamometer and the vibration exciter.

those nonlinear periodic wave in Sec. III B and discuss their experimental relevance in Sec. IV C.

III. MEASUREMENT METHODS

A. Experimental apparatus

The experimental apparatus is sketched in Fig. 3. The system under study is a chain of 51 identical stainless-steel beads [Association Française de Normalisation (AFNOR) norm Z 100 C 17], each 8 mm in diameter, with a tolerance of 4 μm on the diameter and 2 μm on the sphericity, and a maximal roughness of 0.06 μm. The physical properties of the beads are summarized in Table I. The beads are surrounded by a framework of polytetrafluoroethylene (PTFE); this material is chosen because of its high density and low rigidity, leading to a velocity of 400 m/s for bulk acoustic waves, smaller than the velocity of the nonlinear waves observed in our experiments, which is greater than

TABLE I. Relevant physical properties of the beads used in the chain; they are made of stainless steel, corresponding to the AFNOR norm Z 100 C 17.

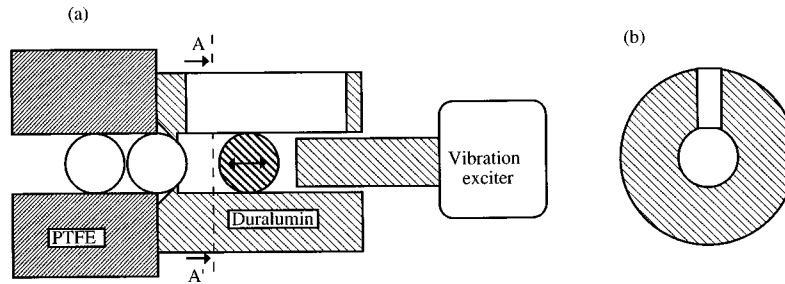| Symbol	Signification	Value
a	bead radius	4 mm $\pm$ 2 μm
E	Young's modulus	2.26×10^{11} N/m^2
ν	Poisson's ratio	0.3
ρ	density	7650 kg/m^3
θ	see Eq. (1)	3.02×10^{-12} m^2/N
$\mathcal{C}$	see Eq. (8)	4.55×10^3 m/s

(a)

(b)

FIG. 4. (a) General sketch of the impact generator. The impacting bead (see Table II for details) moves freely in a hole drilled in a cylinder of duralumin, between the first bead of the chain and a piston mounted on a vibration exciter. (b) Cross section of the cylinder along the plane AA' normal to its axis; this sketch emphasizes the inlet ensuring quick air evacuation, thus a great reduction of air friction on the bead. In the stationary regime, this apparatus send periodically, with the period of the piston motion, (almost) identical nonlinear pulses in the chain.

500 m/s (see Secs. IV B and IV C). The observation of the wave is thus not perturbed by a quicker wave propagating in the surrounding medium. The static force is controlled by a dynamometer, and ranges from 0 to 170 N, with a precision of ± 2 N.

Three force sensors (Dytran™, sensitivity 50 mV/LbF) are held with their axis perpendicular to the chain axis, over beads 6, 26, and 46, allowing the measurement of the wave flight time, but not of its shape. Indeed, those sensors are sensible to the *transverse* deformation of a bead, perpendicular to the direction of propagation of the wave, which is related in a rather complicated manner to the force exerted on the bead by its two neighbors, in the direction of propagation (see [24]). Moreover, the total force is the (algebraic) sum of the forces exerted on each side of the bead and thus related to the *gradient* of the deformation $\psi \equiv -u_\xi$ in the continuous limit. The wave profile is obtained with the help of a fourth force sensor (Dytran™, sensitivity 10 mV/LbF) held at the end of the chain, with its own axis parallel to the chain axis. In this configuration, the force measured by this sensor is related in a simple way to the deformation wave that propagates along the chain [see Eq. (20)]. As shown in Fig. 3, the sensors are linked to a digital scope, suitable for the observation of nonrepetitive pulses; the signal may be transferred to an Apple™ computer for further analysis, to compare the experimental wave profile to the theoretical one (see Secs. IV A and IV C).

The three sensors perpendicular to the chain axis are mounted on brass supports and we monitor the mounting torque with a torque wrench. The last sensor is centered on the chain axis, with its contact surface normal to this axis, and is mounted on a brass cylinder in the same manner as the other three. The cylinder is guided in order to allow the longitudinal displacement of the sensor along the chain axis, required by the settlement of the static force. The dynamometer may press on the brass cylinder, to exert a longitudinal force on the chain, but the contact is not a permanent one and may be broken when no static force has to be applied on the chain. The relevant device, together with the one that allows adjustment of the impact generator, is not shown in Fig. 3.

In order to send high-amplitude compressional waves in the chain, we have built an impact generator sketched in Fig. 4. A bead, contained in a carefully adjusted bore drilled in a duralumin cylinder (an inlet for air evacuation is milled in the cylinder in order to reduce air friction on the bead), moves freely between the first bead of the chain and a dur-

alumin piston held on a Bruel&Kjaer™ vibration exciter. When the piston oscillates, the moving bead successively impacts the piston and the first bead of the chain; for piston oscillation frequencies ranging from 70 to 110 Hz and a free path of several millimeters for the moving bead, the successive impacts occur in a regular fashion. Since the duration of an impact is very small (typically 50 μs; this duration is nevertheless sufficient for the quasistatic approximation to be valid; cf. the beginning of Sec. II), a great amount of momentum may be transferred, generating a maximum amplitude of the wave up to 1200 N (see Sec. IV). In the stationary regime, the period of successive impacts is the same as the one of the piston and is much greater than both the duration of an impact (typically 50 μs) and the time taken by the wave to travel along the chain, which is at least 1 ms in the worst case. The wave is thus completely damped between two successive impacts, mostly because of the very small reflection coefficient at the beginning of the chain, so that two successive pulses do not interact. The amount of impulsion transferred during the impact increases with the amplitude of the piston oscillations, their frequency, the length of the moving bead free path, the restitution coefficient for both impacts experienced by the moving bead, and the density of the moving bead material. Although in a strictly empirical fashion, a proper choice of the parameters listed above allows us to set the amplitude of the traveling pulse to a convenient value. In most cases, the moving bead was made of tungsten carbide and 8 mm in diameter (mass 4 g and a very high restitution coefficient), but we also used other impacting beads listed in Table II.

TABLE II. Characteristics of the different impacting beads used in our experiments. The materials are sorted in decreasing (only in a qualitative sense) restitution coefficient order. The 8-mm tungsten carbide bead was the most frequently used one. This variety of impacting beads allows a large-amplitude range for the pulses sent in the chain.

Impacting bead material	Diameter (mm)	Mass (g)
tungsten carbide	8	3.91
tungsten carbide	12	13.54
bronze	7.95	2.33
stainless steel	8	2.05
duralumin	8	0.71

B. Data analysis

In our experiments we have access to the velocity of the wave, by performing time of flight measurements, and to the time evolution of the force experienced by the sensor held at the end of the chain. The static force applied on the chain is set to a known value with the help of the dynamometer. The actual value of the static force gives the distance of approach δ_0 between two adjacent beads, with the help of Eq. (1), so that

$$\psi_\infty = \frac{\delta_0}{2a} = \frac{\theta^{2/3}}{a^{4/3}} F_0^{2/3}. \qquad (15)$$

Using Eq. (10) we derive a relationship between the unknown quantities y_∞ and V,

$$\psi_\infty = \left(\frac{V}{\mathcal{C}}\right)^4 y_\infty^{4/5}, \qquad (16)$$

where the reader is reminded that the constant $\mathcal{C}$ depends only on the physical properties of the bead material. The maximum amplitude of the solitary wave y_m is a solution of Eq. (13). The definition of $W(y)$ is given by Eq. (11) and we see that Eq. (13) is an algebraic equation of fifth order in the unknown $y_m^{2/5}$; $y_m = y_\infty$ is of course one of the roots and since $dW/dy|_{y_\infty} = 0$ it is a double root. We thus have to solve only a third-order algebraic equation, and we obtain explicitly [25] the function $y_m(y_\infty)$. The unknown y_∞ is thus given by

$$\left[\frac{y_m(y_\infty)}{y_\infty}\right]^{4/5} = \frac{\psi_m}{\psi_\infty}, \qquad (17)$$

where ψ_m is related to y_m by the change of variables (10). The measurement of the maximum force experienced by the force sensor at the end of the chain gives the experimental value of ψ_m. The quantity ψ is the gradient of the *total* displacement of the bead center and is the sum of the constant value at equilibrium $\psi_\infty = \delta_0/2a$ and a time varying part $\widetilde{\psi}(t)$, which is the only part measured by the force sensor. We have to take into account that the contact between the sensor and the last bead of the chain is between a plane and a sphere, so that [9]

$$\delta_{\text{plane-sphere}} = \frac{\delta_{\text{sphere-sphere}}}{2^{1/3}}. \qquad (18)$$

Moreover, the contact surface is at a distance a from the center of the bead. Let x_w be the position of the sensor and δ_w the distance of approach between the sensor and the last bead; we thus have

$$\delta_w \equiv u(x_w - a) - u(x_w) = -a\left(\frac{\partial u}{\partial x}\right)_{x_w} = a\psi. \qquad (19)$$

From this equation we deduce the relationship between the signal given by the sensor $F(t)$, of maximum value F_m, and $\widetilde{\psi}(t)$, which reads

$$\widetilde{\psi}(t) = \frac{\theta^{2/3}}{a^{4/3}} \{[2F(t) + 2F_0]^{2/3} - (2F_0)^{2/3}\}. \qquad (20)$$

We thus get

$$\frac{\psi_m}{\psi_\infty} = \frac{(2F_m + 2F_0)^{2/3} - (2F_0)^{2/3} + F_0^{2/3}}{F_0^{2/3}}. \qquad (21)$$

The knowledge of the applied static force F_0, together with the measurement of the maximum force F_m experienced by the sensor, gives the experimental value of the ratio ψ_m/ψ_∞ from Eq. (21). This value is inserted in Eq. (17), which is solved numerically to obtain the experimental value of y_∞; the numerical root finding is particularly simple here because we know the existence of one and only one root in the range $y_\infty \in [0, (\frac{2}{3})^{5/2}]$ [see in Sec. II the discussion following Eq. (12)]. We then deduce from Eq. (16) the value V of the velocity of the solitary wave predicted by the theory, which may be compared to the observed one (see Sec. IV B).

Introducing the *linear* sound velocity c_s, given by Eq. (6), we may rewrite Eq. (16) as

$$\frac{V}{c_s} = \sqrt{\frac{2}{3}} [y_\infty(F_m/F_0)]^{-1/5}, \qquad (22)$$

where we have emphasized the fact that through Eqs. (21) and (17), y_∞ is a function of the ratio F_m/F_0 only. Thus Eq. (22) means that all the velocity measurements, taken at different applied static forces, may be displayed on a single curve in properly rescaled variables. This is experimentally demonstrated below in Fig. 12.

The theoretical shape of the wave, as measured by the force sensor, may be computed with the help of Eq. (21), which also gives the relationship between $\psi(t) = \widetilde{\psi}(t) + \psi_\infty$ and $F(t)$, and Eq. (10), and reads

$$F(t) = \frac{F_0}{2} \left\{ \left[\left(\frac{y\left(\frac{Vt}{\sqrt{2/5a}}\right)}{y_\infty} \right)^{4/5} - 1 + 2^{2/3} \right]^{3/2} - 2 \right\}, \qquad (23)$$

where the function $y(\eta)$ is obtained by a numerical integration of Eq. (11). The wave shape predicted by Eq. (23) may then be compared to the experimental observations; this is done in Sec. IV A. Note that once F_0 and F_m are known, the theoretical shape of the wave and the theoretical value of its velocity are given without any adjustable parameter.

The case without static force is formally somewhat simpler, in the sense that there is an analytical solution (14) to Eq. (11). However, the physical situation is less clear, and this case deserves particular discussion because the theory predicts propagation of nonlinear *periodic* waves rather than *solitary* waves like in the previous case. The analytic solution (14), together with the relation (20) for the particular case $F_0 = 0$, gives an explicit relation between the velocity of the wave and its maximum amplitude,

$$V|_{F_0 = 0} = \mathcal{C}\left(\frac{4}{5}\right)^{1/2}\left(\frac{2\theta F_m}{a^2}\right)^{1/6}. \qquad (24)$$

The scaling of V with F_m may be understood in a very simple fashion. Let us drop in Eq. (8) the highest derivated terms; we obtain

$$u_{tt} \approx \frac{3}{2} \, \mathcal{C}^2 (-u_x)^{1/2} u_{xx}, \qquad (25)$$

which is a wave equation with an amplitude-dependent wave velocity $V \sim \mathcal{C}(-u_x)^{1/4}$; using Hertz's law (1), we may write $(-u_x) \sim (\theta F_m)^{2/3}/a^{4/3}$, so that we get

$$\frac{V}{\mathcal{C}} \sim \left(\frac{\theta}{a^2}\right)^{1/6} F_m^{1/6}. \qquad (26)$$

In the general case, the velocity depends on both the static force F_0 and the maximal amplitude of the wave F_m, so that this too simple expression has to be corrected to

$$\frac{V}{\mathcal{C}} = \left(\frac{\theta}{a^2}\right)^{1/6} F_m^{1/6} f\left(\frac{F_0}{F_m}\right), \qquad (27)$$

where the function f is only implicitly known, through Eqs. (21), (17), and (16). Formula (24) states that $f(0) = (\frac{4}{5})^{1/2} 2^{1/6}$, and the opposite limit is given by Eq. (6), which states, using the definition of $\mathcal{C}$ in Eq. (8), that $\lim_{F_m \to 0} F_m^{1/6} f(F_0/F_m) = \sqrt{3/2} F_0^{1/6}$.

When no static force is applied on the chain, formula (26) is exact up to a numerical constant. It expresses the fact that the Hertz interaction between adjacent beads is responsible for the propagation of the wave and is a common feature of all waves propagating in that type of medium. For example, the same scaling exists for step waves [19] propagating upward in a chain of beads in contact. The $F_m^{1/6}$ scaling is clearly consistent with experimental observations in Fig. 16, which emphasize that the basic approximations leading to the nonlinear spring-point masses model of Eq. (8) are also valid in the nonlinear regime.

We also stress that although the limit $F_0 \to 0$ is singular for the shape of the wave, because the solitary wave solution disappears, the velocity continuously tends toward expression (24). Indeed, Eq. (11) implies $y_m(y_\infty = 0) = (\frac{5}{4})^{5/2}$, from which we deduce the velocity as a function of ψ_m with Eq. (10) and finally as a function of F_m with the help of Eq. (20), thus recovering Eq. (24). Most probably Eq. (24) is a very good approximation of the solitary wave velocity in the absence of a static force. The shape of the wave, as predicted by this theory, is accurately given by the shape of one arch of the nonlinear periodic wave (14) (see Fig. 2 and the discussion at the end of Sec. II) and reads

$$F(t) = F_m \cos^6 \left(\frac{V|_{F_0=0} \, t}{\sqrt{10}\, a}\right). \qquad (28)$$

IV. EXPERIMENTAL OBSERVATIONS

A. Shape of the wave for nonzero static force

Figure 5 shows a long time recording of the force experienced by the sensor. The pulse corresponds to a compressional wave and exerts only a positive force on the sensor; the oscillations appearing after the arrival of the pulse are
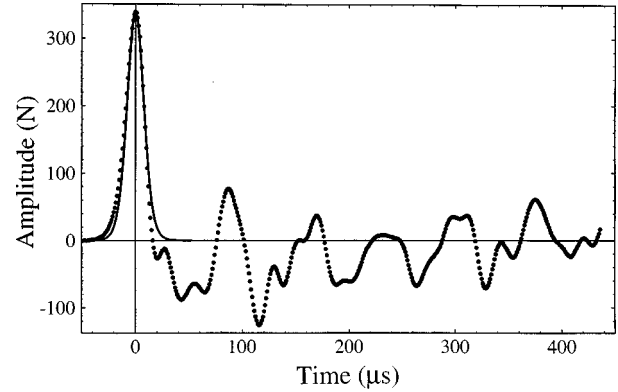

FIG. 5. The dotted curve displays a time recording of the force experienced by the sensor at the end of the chain during a long time, typically 10 times the duration of the first pulse. The abscissa is the time in μs, the ordinate the force in N; the experimental condition are a static force of 167 N and a nonlinear parameter $\psi_m/\psi_\infty = 2.74$. The first positive pulse is identical below with Nesterenko's [14] solitary wave; the solid line shows the theoretical shape of a solitary wave of the same amplitude, derived from Eq. (23). Apart from resonant oscillations of the sensor, we observe an isolated pulse.

due to the resonant response of the sensor (its resonance period is 13 μs, not too far from the duration of the pulse, which is about 50 μs) and multiple reflections in the different parts of the apparatus at the end of the chain.

In Figs. 6–8 we show the experimental shape of the solitary wave recorded by the force sensor at the end of the chain and compare it to the theoretical prediction derived from Eq. (23). The static force is 29.4 N in the case of Figs. 6 and 7 and 167 N for Fig. 8; the available values of the nonlinear parameter ψ_m/ψ_∞ are thus much smaller in this case. Indeed, the nonlinear parameter ranges from 3.7 in Fig. 6(a) to 17.0 in Fig. 7(d), whereas it ranges from 2.5 in Fig. 8(a) to 5.2 in Fig. 8(d), for a range of maximal force experienced by the sensor that is essentially the same for both applied static forces. All the figures exhibit very good agreement with the theory, although the arrival of the pulse seems sometimes slightly different from the theoretical expectations. It is important to note that in this test of the theory *no* adjustable parameter is involved.

The typical duration of a pulse is about 30–40 μs and its velocity is about 1000 m/s; the typical length scale of a pulse is thus 3–4 cm or 4–5 beads. The long-wavelength approximation (7) is thus fulfilled and the pulse propagates on a range much greater than its spatial extension, so that we can indeed call it a solitary wave. Another general conclusion that may be drawn is that in all cases the duration of the pulse is much greater than the time taken by a bulk acoustic wave to travel across a bead diameter, which is a necessary condition to apply Hertz's theory to a nonstatic situation.

B. Velocity of the wave for nonzero static force

We give below experimental results on pulse propagation in the chain for three different values of the applied static force: 9.8$\pm$1, 29.4$\pm$1, and 167$\pm$1 N. An important parameter to consider is the ratio ψ_m/ψ_∞, given by Eq. (21) in term of the static and dynamic forces, which characterize the
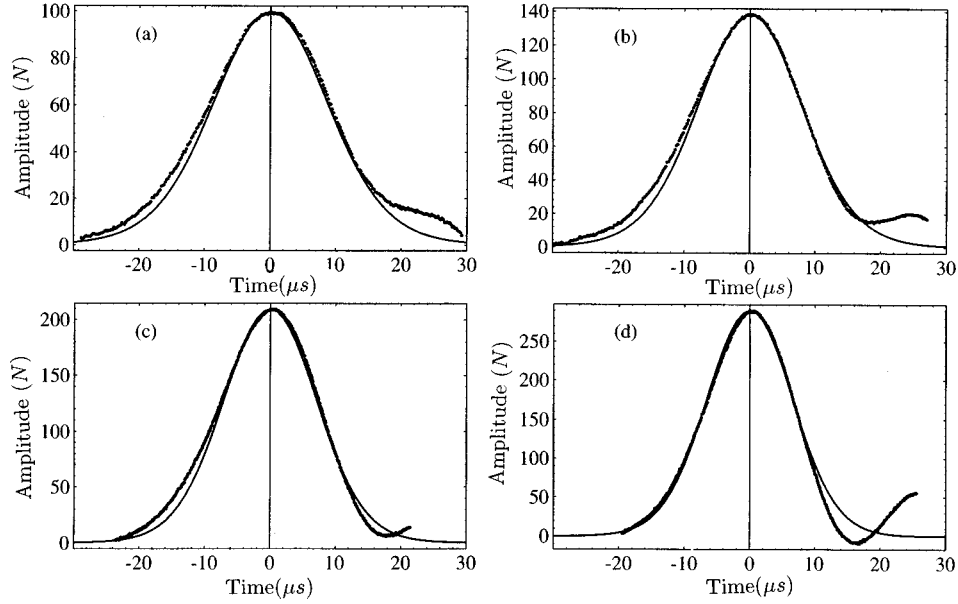
FIG. 6. Shape of four different solitary waves recorded at the end of the chain, for a static force of 29.7 N. Each graph displays the evolution of the force (in N) with time (in μs). The dots are experimental points, whereas the solid lines are the theoretical predictions derived from Eq. (23). We give in each case the maximum amplitude F_m, the velocity V, and the nonlinear parameter ψ_m/ψ_∞ of each wave: (a) $F_m = 100$ N, $V = 895$ m/s, $\psi_m/\psi_\infty = 3.7$; (b) $F_m = 138$ N, $V = 921$ m/s, $\psi_m/\psi_\infty = 4.5$; (c) $F_m = 209$ N, $V = 960$ m/s, $\psi_m/\psi_\infty = 5.8$; and (d) $F_m = 290$ N, $V = 994$ m/s, $\psi_m/\psi_\infty = 7.2$.

nonlinearity of the wave. This ratio must be much greater than 1 in order that Eq. (8) be valid; in our experiments, we have

$$\psi_m/\psi_\infty \in [1.9, 17.0] \quad \text{for } F_0 = 9.8 \text{ N,}$$

$$\psi_m/\psi_\infty \in [1.4, 16.5] \quad \text{for } F_0 = 29.4 \text{ N,} \quad (29)$$

$$\psi_m/\psi_\infty \in [1.5, 5.2] \quad \text{for } F_0 = 167 \text{ N.}$$

We obtain the wave velocity very simply from time-of-flight measurements between the four sensors available along

the chain (see the details on the experimental apparatus in Sec. III A). As we stressed before, the three force sensors that are held perpendicularly to the chain are well suited for such types of measurements, although they give no information about the actual shape of the wave. The theoretical value of the wave velocity is derived as explained in Sec. III B, with *no* free parameter once the applied static force and the maximal amplitude of the wave are both known.

We show in Figs. 9–11 the results of wave velocity measurements for static forces of, respectively, 9.8, 29.7, and 167 N. For the two smallest static forces, there is good agree-
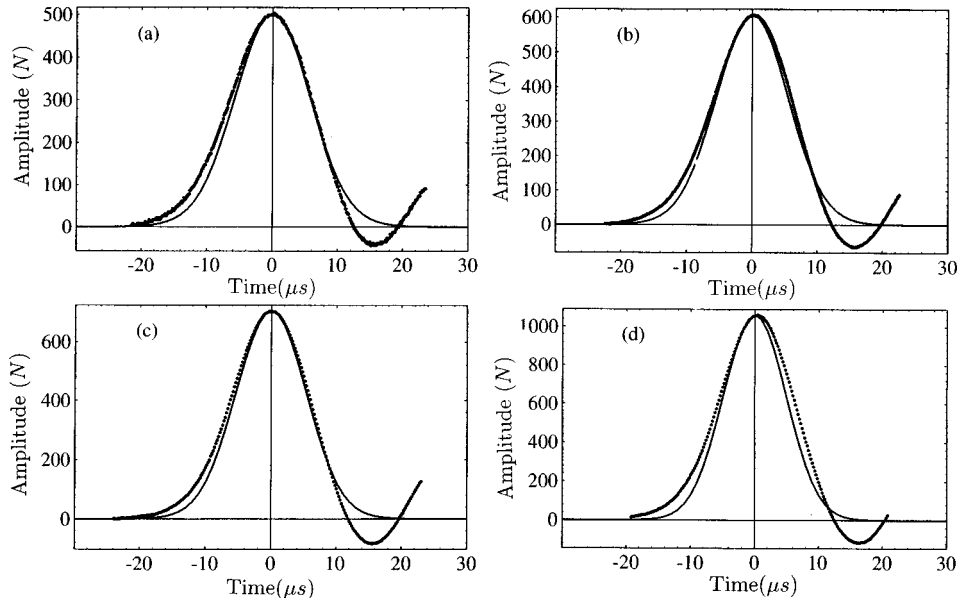
FIG. 7. Same as Fig. 6, with the same notations, but for greater values of ψ_m/ψ_∞. The respective characteristics of each pulse are (a) $F_m = 503$ N, $V = 1060$ m/s, $\psi_m/\psi_\infty = 10.4$; (b) $F_m = 608$ N, $V = 1086$ m/s, $\psi_m/\psi_\infty = 11.8$; (c) $F_m = 705$ N, $V = 1106$ m/s, $\psi_m/\psi_\infty = 13.0$; and (d) $F_m = 1060$ N, $V = 1168$ m/s, $\psi_m/\psi_\infty = 17.0$.
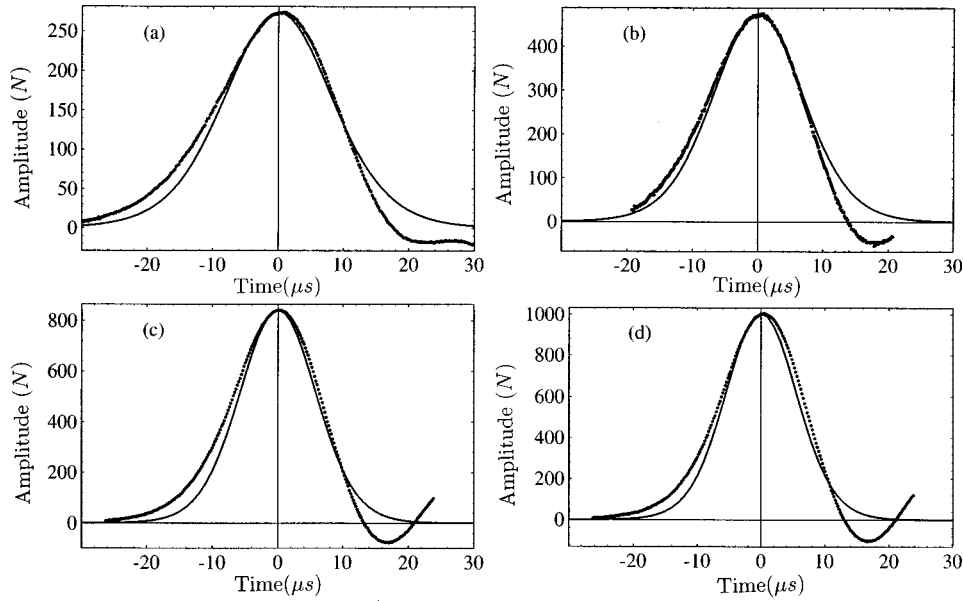
FIG. 8. Same as Fig. 6, with the same notations, but for a static force of 167 N. The respective characteristics of each pulse are (a) $F_m = 274$ N, $V = 1131$ m/s, $\psi_m/\psi_\infty = 2.5$; (b) $F_m = 474$ N, $V = 1178$ m/s, $\psi_m/\psi_\infty = 3.3$; (c) $F_m = 842$ N, $V = 1239$ m/s, $\psi_m/\psi_\infty = 4.7$; and (d) $F_m = 1005$ N, $V = 1260$ m/s, $\psi_m/\psi_\infty = 5.2$.

ment between the theoretical predictions and the measurements. In each case the nonlinear parameter ranges between the same limits, as shown by Eq. (29). A small discrepancy is shown by the measurements at 167 N; a possible explanation is an increase of energy transfer between the wave and the framework containing the beads, due to the high static force. A wave arriving at the end of the chain has lost energy and has thus propagated quicker than what is predicted from its final amplitude; this interpretation is supported by the good agreement of the experimental and theoretical shape of the wave at the same static force shown in Fig. 8. If the discrepancy was due to the smallness of the nonlinear parameter [see Eq. (29)], it should have been exhibited in Fig. 8 too. The successive time-of-flight measurements along the chain do display some scattering of the data, hence the error

bars of the graphs. The accuracy of the data is not sufficient to observe a systematic evolution of the velocity, which seems rather constant during the pulse propagation, even for a static force of 167 N.

As we explained above, in the paragraph following Eq. (22), the measurements of Figs. 9–11 may be displayed on a single curve when expressed in rescaled variables V/c_s and F_m/F_0. This is demonstrated in Figs. 12(a) and 12(b). Figure 12(a) shows that all the previous data lie on a single curve, when expressed in the variables V/c_s and F_m/F_0. Figure 12(b) shows that, as predicted by Eq. (22), V/c_s is indeed a linear function of $[y_\infty(F_m/F_0)]^{-1/5}$. A fit of the proportionality constant gives 0.84, which compares well with the expected value $\sqrt{2/3} \approx 0.8165$. Note also that Fig. 12 clearly shows that the nonlinear waves are *supersonic*, a result predicted by Nesterenko [14].

C. The case of zero static force

In order to be experimentally as close as possible to the case of zero static force, we proceed in the following man-
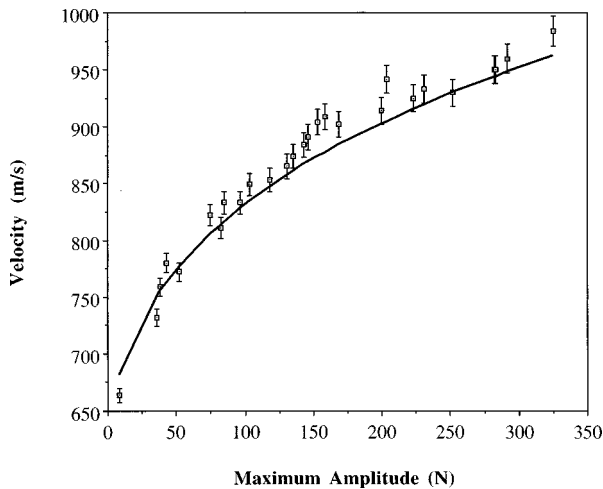

FIG. 9. Evolution of the wave velocity (in m/s) with the maximum amplitude of the wave (in N) for an applied force of 9.8 N. The solid line is the theoretical prediction, derived from Eqs. (21), (17), and (16).
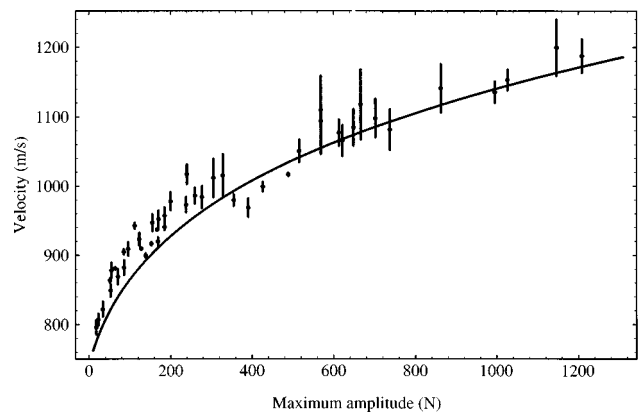

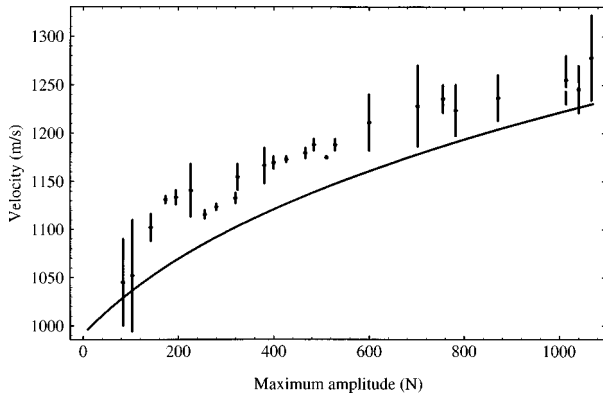FIG. 10. Same as Fig. 9, but for an applied static force of 29.7 N.

FIG. 11. Same as Figs. 9 and 10, but for an applied static force of 167 N.

FIG. 12. (a) Plot of the dimensionless ratio V/c_s versus the dimensionless quantity F_m/F_0. The data are represented by circles for a static force of 29.7 N, by triangles for a static force of 9.8 N, and by squares for a static force of 167 N. All the experimental points lie on a single curve. The solid line is the curve const $\times[y_\infty(F_m/F_0)]^{-1/5}$, where the experimental value of the constant is 0.84. This is to be compared with the theoretical prediction (22) in which const$=\sqrt{2/3}\approx0.8165$. (b) Plot of the dimensionless ratio V/c_s versus the dimensionless quantity $[y_\infty(F_m/F_0)]^{-1/5}$, with the same symbols as before. The data all lie on a single *linear* curve, whose slope is found to be const$=0.84$.

ner. We exert a static force on the chain in order to set the beads into contact and then we relax this force until the contact between the dynamometer and the brass cylinder that support the longitudinal force sensor is broken. There is almost no adhesion between the steel beads, but there may be some uncontrolled friction with the walls of the channel containing the beads. We expect this friction to be small for smooth steel beads in contact with PTFE. Experimentally, the static force between two adjacent beads is certainly very small, but we cannot be sure that it is strictly zero. In that sense, the singularity of the zero static force case is rather a mathematical oddity than an actual physical effect.

When no static force is applied to the chain, the theory predicts the propagation of nonlinear periodic waves rather than solitary waves as in the previous case. We have recorded the shape of the pulses arriving at the end of the chain in a large range of amplitudes, from 40 to 700 N. Experimentally, the comparison of the Figs. 6–8 with Figs. 13–15 proves that there is no qualitative difference between the cases of zero and nonzero static force. Concerning the shape of the wave, as it is clearly demonstrated in Fig. 2, it is not possible to distinguish a solitary wave in the limit of very small static force from an arch of the nonlinear periodic wave. In Figs. 13–15 we compare the experimental shape of a pulse to one arch of a solution (28) with the same maximal amplitude for different values of the maximal amplitude of the pulse. The agreement between the observed shape of the pulse and the theoretical prediction is striking, except for the smallest amplitude pulses displayed in Fig. 13. The duration [26] of the pulse is about 30 μs and its velocity is about 900 m/s. The spatial extension of the pulse is then about 30 mm, roughly four beads, which is enough to ensure the validity the long-wavelength approximation (7). Indeed, one knows from numerical simulations [27] that in discrete nonlinear chains, the excitations are perfectly described by the continuous approximation if their size is greater than or equal to five particles. This length is also much less than the total length of the chain, which means that the pulse has kept its shape over a great distance, as a solitary wave should. The difference from the previous case of Sec. IV A is that we are in the fully nonlinear regime, so that the development (8) is certainly correct.

As shown in Fig. 13, the agreement between the shape of the pulse and the theoretical prediction becomes poor for an amplitude roughly less than 70 N. A possible interpretation
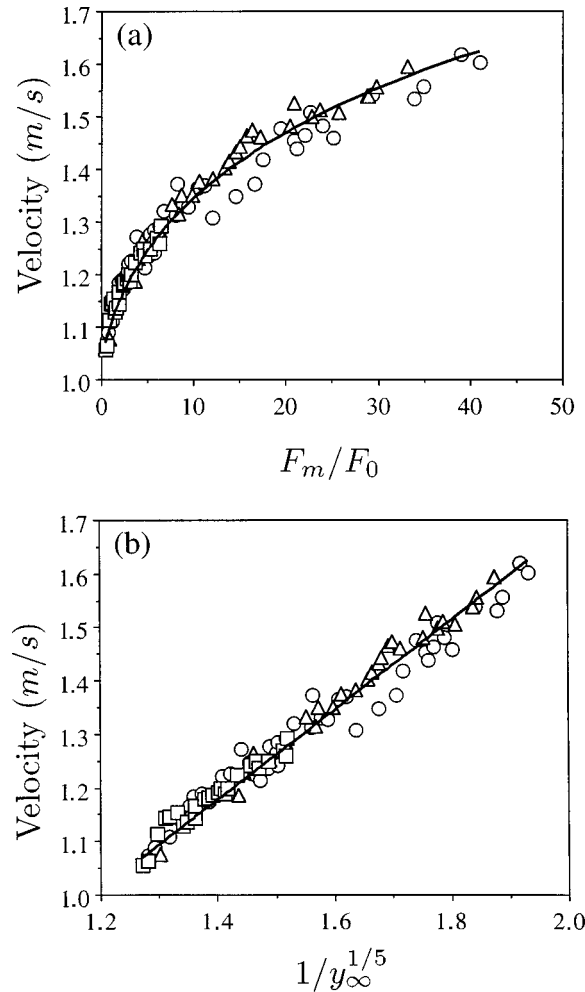
for the discrepancy between the observed shape of the pulses and the predicted one could be that the friction of the beads on the walls causes a residual static force $F_0^*>0$. But any order of magnitude derived from Fig. 8, e.g., will give for F_0^* a value much too high to be accepted. Another possibility is that, at low impact amplitude, it takes too much time for the pulse to reach its asymptotic shape (i.e., the solitary wave profile) from the initial wave profile. Unfortunately, there is no theoretical information about the times taken by a given profile to reach its asymptotic shape and we are unable to test this interpretation. We stress that the amplitudes of the waves in those experiments are much smaller than in the experiments reported in Sec. IV A, in which this effect was not observed.

From the pulse velocity measurements, we can first verify that $V|_{F_0=0}$ scales as $F_m^{1/6}$; Fig. 16 shows that this is indeed
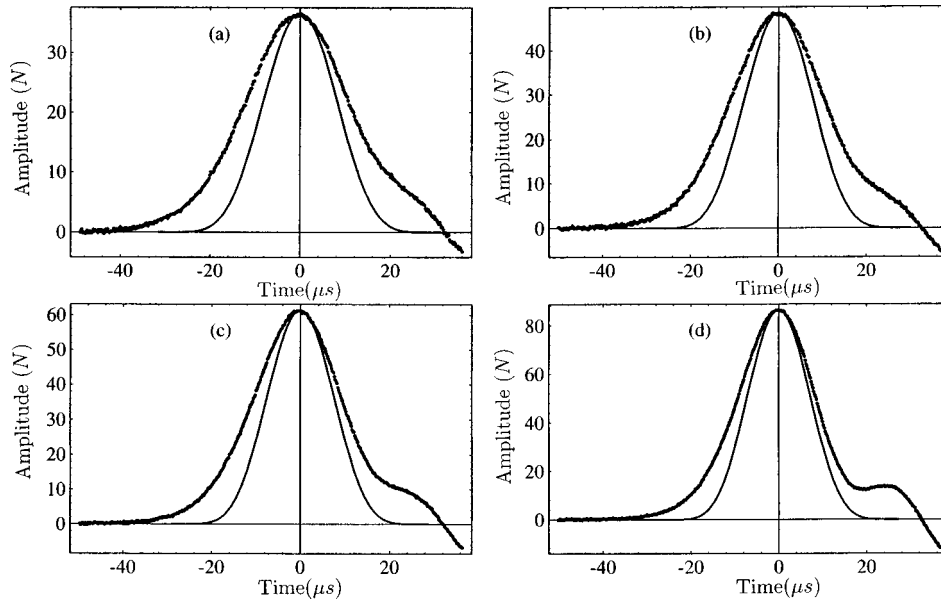
FIG. 13. Shape of the pulse at the end of the chain, when no static force is applied to the chain. Each graph displays the evolution of the force (in N) with time (in μs). Dots are experimental values recorded by the digital scope and solid lines the theoretical prediction (28) for a wave of the same maximal amplitude. The velocities and amplitudes of the pulses are, respectively, (a) $V=629$ m/s, $F_m=36.7$ N; (b) $V=659$ m/s, $F_m=48.5$ N; (c) $V=685$ m/s, $F_m=61.4$ N; and (d) $V=725$ m/s, $F_m=86.4$ N. The pulses are of small amplitude and the agreement with the theory is rather poor, except for the highest amplitude pulse displayed in (d).

the case. This result indicates that the Hertz interaction (1), in the quasistatic approximation (8), fully accounts for the propagation of the pulse in the nonlinear regime too [see the discussion above Eq. (26)]. Like in the previous case, no systematic evolution of the velocity with the travel time of the pulse is observed. In Fig. 17 we show that formula (24) gives rather accurately the velocity of the pulse. This behavior is linked to the fact that the solitary wave velocity tends continuously toward Eq. (24) in the $F_0 \rightarrow 0$ limit, as we showed in Sec. III B.

Even in the case of zero static force applied to the chain, we observe pulses that propagate over a great distance, with a constant velocity and shape, so that they may be identified with *solitary waves*. Their velocity and shape are both in fair agreement with the theoretical predictions of Nesterenko [14,15] if we forget that in this singular limit nonlinear periodic waves are predicted rather than solitary waves. Of course the impact generator is not well suited to generate periodic waves and we cannot expect this type of wave to appear spontaneously. Within the precision of our measure-
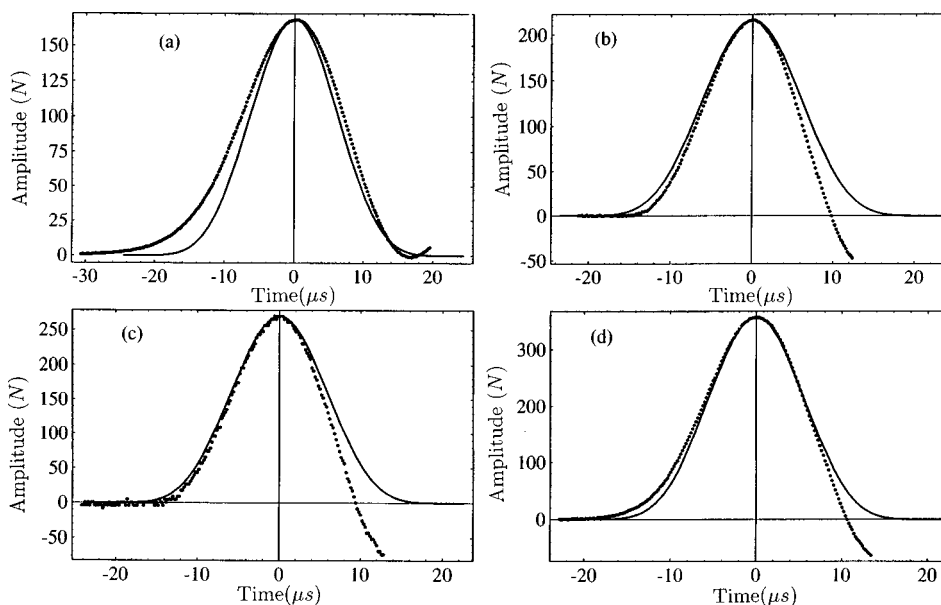

FIG. 14. Same as Fig. 13, but for waves of greater amplitudes. The velocities and amplitudes of the pulses are, respectively, (a) $V=811$ m/s, $F_m=168.5$ N; (b) $V=845$ m/s, $F_m=216.2$ N; (c) $V=877$ m/s, $F_m=269.7$ N; and (d) $V=919$ m/s, $F_m=356.4$ N. The negative part of the force signal at the back of the pulses in (b)–(d) is the signature of the sensor resonance. The agreement with the theory is very satisfactory and much better than for the pulses of Fig. 13.
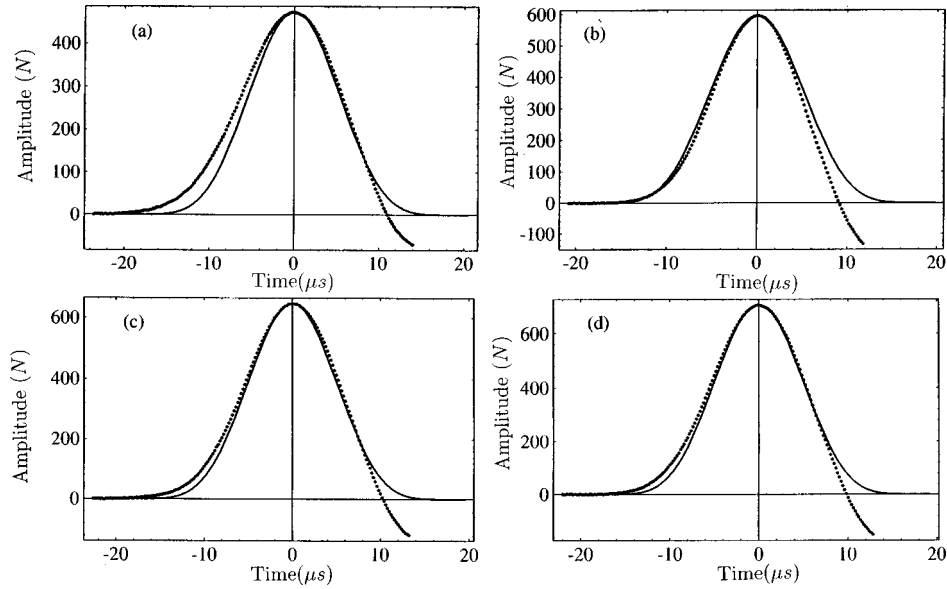
FIG. 15. Same as Figs. 13 and 14, but for waves of greater amplitudes. The velocities and amplitudes of the pulses are, respectively, (a) $V = 963$ m/s, $F_m = 473.1$ N; (b) $V = 1000$ m/s, $F_m = 594.0$ N; (c) $V = 1014$ m/s, $F_m = 646.1$ N; and (d) $V = 1029$ m/s, $F_m = 704.6$ N. The negative part of the force signal at the back of the pulse is the signature of the sensor resonance. As in Fig. 14, the agreement with the theory is very good.

ments, the pulses are able to travel more than ten times their length while keeping their shape and velocity, which means that they are rather stable.

D. Discussion

In this section, we compare our results to the previous experiments of Nesterenko and Lazaridi [16–18]. They have observed the propagation of wave trains, built of several solitary waves, in chains of steel beads with zero applied static force. The initial impact was much more violent in their experiments (the impacting mass was five times that of a bead in the chain and its velocity 1 m/s, more than twice what we get in our experiments), which explains that several

solitary waves were generated. Moreover, they did not vary the intensity of the first impact. They have also conducted similar experiments [17,18] with applied static forces of 2 and 20 N. An interesting result is that the pulses observed with a static force of 2 N are almost identical to the ones observed without static compression of the chain; moreover, this behavior is confirmed by numerical simulations.

They recorded the arrival of the wave train at the end of the chain and compared its shape with numerical simulations that included *the impact on the first bead of the chain* with the colliding mass used to generate the wave train. The velocity of the first pulse was not measured, but the time intervals between successive pulses, together with their respective amplitudes, compared well with the theoretical expectations for a short chain of 20 beads; the agreement was only qualitative for a longer chain of 40 beads. In either cases, the
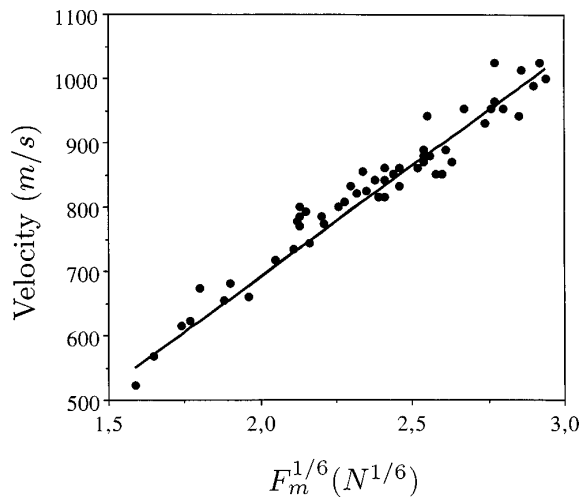

FIG. 16. Graph of the wave velocity (in m/s) as a function of $F_m^{1/6}$ (in N$^{1/6}$), where F_m is the maximum amplitude of the wave, when no static force is applied on the chain; the relation is clearly linear, which simply states that the Hertz interaction between adjacent beads is responsible for wave propagation.
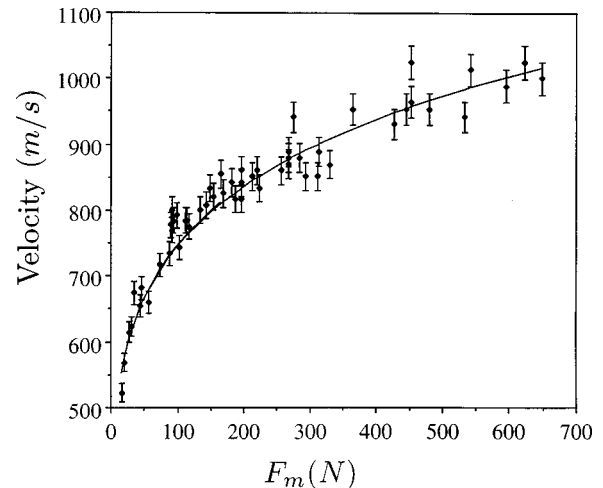

FIG. 17. Evolution of the wave velocity (in m/s) with the maximum amplitude of the wave F_m (in N) for no applied static force. The solid line is the theoretical prediction (24).

comparison between the shape of the pulses was only qualitative.

Our experimental setup allows the exploration of a large range in the amplitude of the pulses, roughly from 1 to 20, and permits a systematic study of the shape and velocity of the waves as functions of their maximum amplitude. In our experiments, the chain contains 51 beads, and we find excellent agreement with the theory for either the velocity of the pulses or their *complete* shape. We do not confirm the strong attenuation of the wave reported by Nesterenko and Lazaridi for the long chain of 40 beads.

A possible interpretation of this discrepancy is as follows. In their experiments, the beads are 4.75 mm in diameter, contained in a quartz tube with an inside diameter of 5 mm. The beads are thus allowed to move rather easily away from the tube axis and presumably they lose a lot of energy in impacting the tube; this effect is reinforced if the length of the chain is increased. In our experiments, the beads are contained in a channel drilled in a framework of PTFE, with a very small clearance of $\frac{2}{100}$ mm. Impacts on the walls are suppressed and, moreover, the acoustic coupling between steel and PTFE is much smaller than between steel and quartz.

V. CONCLUSIONS

We have conducted experiments on a chain of identical beads in contact with either moderate static forces or zero static force applied to the chain. With the help of an impact generator, we were able to generate high-amplitude pulses in the chain, that is, with a dynamical amplitude much higher than the static force.

With our experimental setup we were able to vary the static force applied on the chain, together with the pulses amplitude. We added to the previous work of Nesterenko and Lazaridi [16–18] a systematic and quantitative study of the velocity and shape of the solitary waves.

At the end of the chain, we recorded the time evolution of the force exerted on a dynamic force sensor and compared this experimental shape of the pulse with the theoretical predictions of Nesterenko [14,15]. The agreement was very good when no static force was applied on the chain, except for excitations of very small amplitude; with a nonzero static force, excellent agreement was found between theoretical predictions and experimental observations. In all cases, no adjustable parameter was involved in the data analysis.

The velocity of the pulse seems to be accurately predicted by the theory, either with or without static force applied on the chain. Velocity measurements for different nonzero applied static forces may be displayed on a single curve with proper rescaling of the variables. We stress that, as for the pulse shape, no adjustable parameter has been used.

In all cases, the typical size of the excitation is about four or five beads, which is sufficient to ensure the validity of a long-wavelength approximation. This size is also about one-tenth of the total length of the chain, which means that the pulses propagate over a large distance while keeping their velocity and shape. This is strong experimental evidence of nonlinear solitary wave propagation in a chain of beads in Hertzian contact, even in the limit of zero applied static force.

[1] K. Iida, Bull. Earthquake Res. Inst. (Tokyo) **16**, 131 (1938).

[2] K. Iida, Bull. Earthquake Res. Inst. (Tokyo) **17**, 783 (1939).

[3] J. D. Goddard, Proc. R. Soc. London, Ser. A **430**, 105 (1990).

[4] P. Talwani, A. Nur, and R. L. Kovach, J. Geophys. Res. **78**, 6899 (1973).

[5] C. W. Thurston and H. Deresiewicz, J. Appl. Mech. ASME **26**, 251 (1959).

[6] N. Warren and O. L. Anderson, J. Geophys. Res. **78**, 6911 (1973).

[7] Chu-heng Liu and S. R. Nagel, Phys. Rev. Lett. **68**, 2301 (1992).

[8] Chu-heng Liu and S. R. Nagel, Phys. Rev. B **48**, 15 646 (1993).

[9] L. D. Landau and E. M. Lifshitz, *Theory of Elasticity* (Pergamon, Oxford, 1986).

[10] C. Coste, E. Falcon, and S. Fauve, in *Des Géomatériaux aux Ouvrages*, edited by C. Petit, G. Pijaudier-Cabot, and J.-M. Reynouards (Hermes, Paris, 1995).

[11] T. G. Hill and L. Knopoff, J. Geophys. Res. **85**, 7025 (1980).

[12] D. F. Strenzwilk, J. Appl. Phys. **50**, 6767 (1979).

[13] D. H. Tsai and C. W. Beckett, J. Geophys. Res. **71**, 2601 (1966).

[14] V. F. Nesterenko, J. Appl. Mech. Tech. Phys. (USSR) **5**, 733 (1984).

[15] V. F. Nesterenko, J. Phys. IV **55**, C8-729 (1994).

[16] A. N. Lazaridi and V. F. Nesterenko, J. Appl. Mech. Technol. Phys. (USSR) **26**, 405 (1985).

[17] V. F. Nesterenko and A. N. Lazaridi, in *Problems of Nonlinear Acoustics*, Proceedings of the IUPAP, IUTAM Symposium on Nonlinear Acoustics, edited by V. K. Kedrinski (Nauka, Novosibirsk, 1987), Vol. 1, pp. 309–313.

[18] V. F. Nesterenko, *High-Rate Deformation of Heterogeneous Materials* (Nauka, Novosibirsk, 1992).

[19] E. Falcon, C. Laroche, S. Fauve, and C. Coste (unpublished).

[20] R. S. Sinkovits and S. Sen, Phys. Rev. Lett. **74**, 2686 (1995).

[21] K. L. Johnson, *Contact Mechanics* (Cambridge University Press, Cambridge, 1992).

[22] J.-M. Hertzsch, F. Spahn, and N. V. Brilliantov, J. Phys. II **5**, 1725 (1995).

[23] S. L. Gavrilyuk and V. F. Nesterenko, Prikl. Mekh. Tekh. Fiz. **6**, 45 (1993).

[24] K. Walton, Geophys. J. R. Astron. Soc. **43**, 293 (1975).

[25] We do not display the relevant cumbersome expression, which may be found with a formal calculus software such as MATH-EMATICA.

[26] Note that this time scale is fully compatible with the quasi-static approximation.

[27] M. Peyrard and M. D. Kruskal, Physica D **14**, 88 (1984).